Strojnícky časopis – Journal of MECHANICAL ENGINEERING,
VOL 76 (2026), NO 2, 112 – 123

# NUMERICAL MODELING AND PARAMETRIC OPTIMIZATION OF THE PRESS PLATE FOR THE GLASS COMPARTMENT OF A THREE-COMPARTMENT REFUSE COLLECTION VEHICLE WITH VARIABLE COMPARTMENT VOLUMES

**KIZDARBEKOVA Makpal[1], SAVINKIN Vitaliy[1*], BALABEKOVA Kyrmyzy[2*], ALIPBAYEV Zhasulan[2*]**

*[1]Department of Transport and Mechanical Engineering, Faculty of Engineering and Digital Technology, M. Kozybayev North Kazakhstan University, 86 Pushkin St., Petropavlovsk 150000, Kazakhstan, e – mail: cavinkin7@mail.ru*
*[2]Transport and Energy Faculty, Department of Transport Engineering of L.N.Gumilyov Eurasian National University, Kazhymukan str. 13 build, 424 of, 010008, Astana, Kazakhstan, e – mail: balabekovakyrmyzy@enu.kz , alipbayevzhasulan@enu.kz*

**Abstract:** A coupled discrete-element/finite-element (DEM-FEA) framework was applied to evaluate and optimize the press plate of the glass compartment in a three-compartment refuse collection vehicle with variable compartment volumes. Contact loading generated during a 0.6 m compaction stroke was obtained in Ansys Rocky and transferred to Ansys Mechanical for static structural analysis. The baseline design produced a maximum Z-direction displacement of -10.8 mm and a maximum von Mises stress of 229.88 MPa, exceeding the adopted limits of 8 mm and 196 MPa. Three design variables were considered: main-plate thickness t, hydraulic-strut attachment position a, and stiffening-rib thickness b. A response-surface model based on Non-Parametric Regression was used for parametric optimization. Three feasible candidate designs were obtained. The lightest candidate had t = 14.936 mm, a = 283.02 mm, b = 36.877 mm, a stress of 146.81 MPa, a mass of 1072.2 kg, and a displacement of -7.483 mm. The results demonstrate that DEM-derived loading combined with FEA and surrogate-based optimization can support rational press-plate design, although experimental calibration of contact parameters and verification of load transfer remain necessary before production implementation.

**Keywords:** press plate, three-compartment refuse collection vehicle, separate waste collection, glass waste, Ansys Rocky, DEM, Ansys Mechanical, FEA, response surface, Non-Parametric Regression, parametric optimization, 09G2S steel

## 1 Introduction

Separate waste collection places new requirements on refuse collection vehicle design because individual waste fractions differ in density, compressibility, particle geometry, and compaction behavior. A three-compartment body with movable press plates and operationally variable compartment volumes can improve utilization of the available body space when the amounts of plastic, paper, and glass are unequal [9]. At the same time, the movable partitions and press plates become load-bearing elements whose strength and stiffness directly affect the reliability of the compaction and unloading cycle.

Glass waste is particularly demanding because its high density and irregular particle shape generate strongly nonuniform contact forces during compaction. Replacing these forces with a single uniform pressure is convenient for preliminary calculations but may distort the local stress state when plate thickness, stiffening ribs, and support positions are being optimized. The discrete element method (DEM) is appropriate for such granular media because it explicitly represents particle motion and contact interaction [1, 2]. Industrial implementations such as

DOI: 10.2478/scjme-2026-0025, Print ISSN 0039-2472, On-line ISSN 2450-5471
© This is an open access article licensed under the Creative Commons Attribution-NonCommercial-NoDerivatives License (http://creativecommons.org/licenses/by-nc-nd/4.0/).

Ansys Rocky also allow contact loads obtained from DEM simulations to be transferred to Ansys Mechanical for structural analysis [3, 4].

For computationally expensive coupled models, response-surface and surrogate techniques reduce the number of repeated high-fidelity analyses required during optimization [5-7]. Their usefulness is particularly relevant when the structural response is nonlinear with respect to geometric variables. However, the quality of a metamodel does not by itself guarantee physical validity: DEM contact coefficients, the mapping of pressure to the finite-element model, mesh sensitivity, and boundary conditions must remain consistent with the actual mechanism.

Patent and utility-model solutions for refuse collection and compaction systems confirm the practical relevance of movable hydraulic elements, partitions, and discharge devices [8, 9]. The design considered in this study changes the volumes of the side and central compartments and uses a two-cycle unloading procedure. This functional concept is shown in Fig. 1 and provides the design basis for the numerical analysis.

The aim of this study is to numerically evaluate and parametrically optimize the press plate of the glass compartment using a coupled DEM-FEA framework. Three design variables are considered: main-plate thickness t, hydraulic-strut attachment position a, and stiffening-rib thickness b. Their influence on maximum von Mises stress, Z-direction displacement, and structural mass is evaluated to identify a design that satisfies the adopted strength and stiffness constraints at minimum mass.

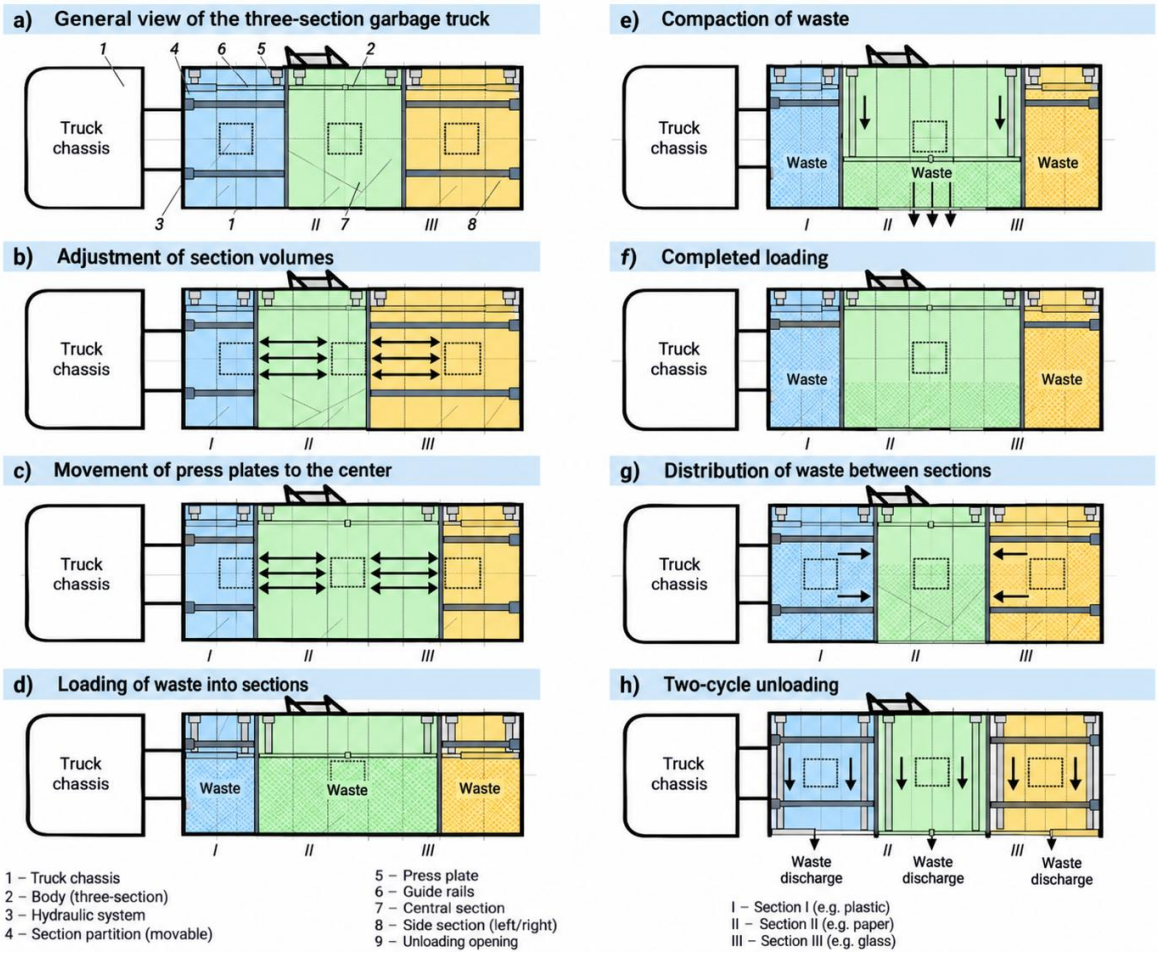



Fig. 1 Separate collection, compaction, redistribution, and unloading concept for the variable-volume three-compartment refuse collection vehicle

## 2 Materials and Methods

### 2.1 Design basis and material

The vehicle body is divided into three compartments intended for different waste fractions. Movable central press plates allow the useful volumes of the side compartments to vary by approximately 30% and that of the central compartment by approximately 60% relative to the base configuration [9]. During operation, the plates compact the loaded waste and participate in the unloading cycle; therefore, excessive deformation may impair plate motion, increase guide wear, or cause jamming.

The geometric parameterization of the analyzed plate is shown in Fig. 2. The main-plate thickness is denoted by t, the hydraulic-strut attachment position by a, and the stiffening-rib thickness by b. These variables were selected because they have a direct and interpretable influence on bending stiffness, reaction-force transfer, local reinforcement, and structural mass.

The press plate was modeled as 09G2S steel. The principal properties used in the calculations are summarized in Table 1. An allowable equivalent stress of 196 MPa was adopted as the strength constraint. This value is conservative relative to the reported yield-strength range and was retained because the loading originates from a particle-contact model that still requires experimental calibration.

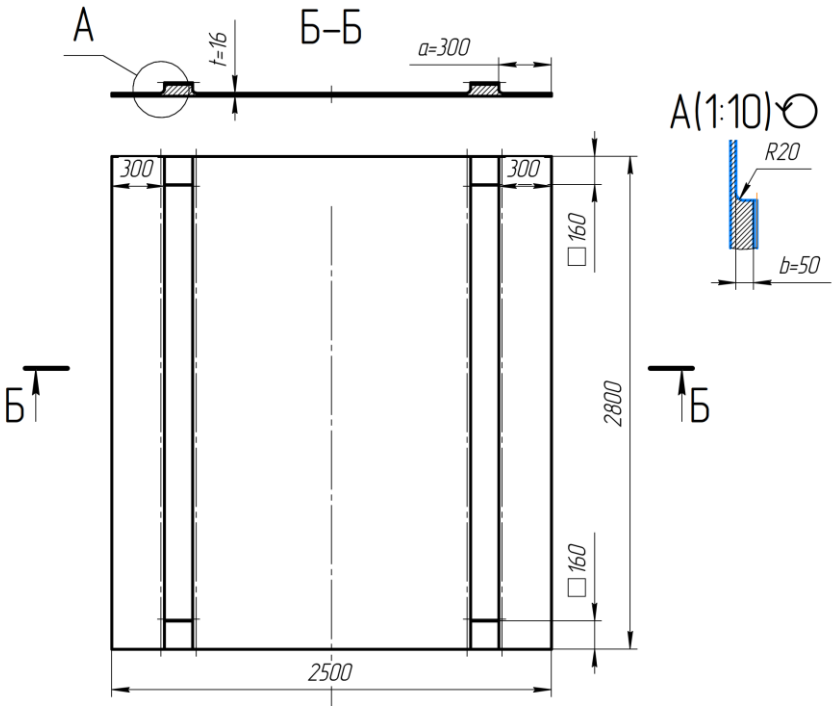



Fig. 2 Geometric scheme of the press plate and design parameters t, a, and b

Table 1. Principal design properties of 09G2S steel

| Parameter | Adopted value |
|---|---|
| Elastic modulus E | 2.0-2.1×10⁵ MPa |
| Poisson's ratio | 0.3 |
| Density | 7850 kg/m³ |
| Allowable stress | 196 MPa |

## 2.2 Supplementary model of compartment filling, waste compaction, and hydraulic drive

To complement the structural optimization of the glass-compartment press plate, the extended mathematical formulation considers how the loading conditions may depend on the filling and compaction behaviour of different waste fractions. The following relations are an analytical modelling framework introduced in the extended manuscript; they were not independently validated by the DEM-FEA calculations reported in Section 3. In particular, no new simulation-derived optimum hydraulic pressure or power consumption is claimed.

### 2.2.1 Compartment volume and filling dynamics

For a three-compartment body, the material indices are i ∈ {G, P, T}, denoting glass, paper/cardboard, and tinplate waste, respectively. The model characterizes each compartment by its length Li, width Bi, height Hi, geometric shape factor, and time-dependent filling coefficient. The nominal volume is:

$$V_i^0 = L_i \cdot B_i \cdot H_i i \in \{G, P, T\} \quad (1)$$

The effective occupied volume is represented by the product of nominal volume, filling coefficient ηi(t), and geometric correction factor ki,geom:

The dynamic filling balance accounts for material input qi,in(t), a characteristic compaction time Ti,comp, and threshold-controlled activation of compaction through the Heaviside function Θ:

This relationship is intended to describe time-varying available space during loading and compression; it requires calibration of flow rates, compaction time, and activation threshold before operational predictions can be made.

### 2.2.2 Density and compression of different waste fractions

The source model relates the evolving bulk density ρi(t) to pressure p(t) using dimensionless empirical coefficients αi and βi and reference pressure pi,ref:

The extended version gives illustrative coefficient pairs αG ≈ 0.8, βG ≈ 0.6 for brittle glass, αP ≈ 2.5, βP ≈ 0.4 for the elastoplastic response of paper, and αT ≈ 1.5, βT ≈ 0.5 for plastically deforming tinplate. These coefficients are provisional assumptions, not experimentally verified material constants.

Table 2a. Initial bulk-density and compaction-ratio ranges reported in the extended formulation

| Waste fraction | Initial bulk density (kg/m³) | Compaction ratio |
|---|---|---|
| Glass | 300–500 | 2–3 |
| Paper/cardboard | 60–120 | 4–7 |
| Tinplate | 100–200 | 3–6 |

The listed ranges are modeling inputs supplied by the extended draft; their provenance and applicability to the actual waste stream must be checked. Material mass and effective occupied volume are related by:

The corresponding mass-balance relation describes the accumulation of incoming material, while the effective compacted volume follows from mass divided by the evolving bulk density:

The compaction ratio can therefore be described using initial and current densities. Unlike the DEM representation of glass fragments, this lumped model does not reproduce local force chains, particle breakage, or the spatial heterogeneity of pressure on the plate.

### 2.2.3 Hydraulic actuation and resisting load

For the hydraulic compaction drive, let ph(t) be hydraulic pressure, Qh(t) the working-fluid flow rate, Ap the piston area, and ηm and ηv mechanical and volumetric efficiencies. The idealized actuator force and piston speed are written as:

$$F(t) = ph(t) \cdot A_p \cdot \eta_m \tag{2}$$

$$v_p(t) = \frac{Q_h(t)}{A_p} \cdot \eta_v \tag{3}$$

The dynamic force balance accounts for piston-system inertia and opposing forces produced by compressed waste, friction, and other inertial effects:

In the source formulation, material-dependent resisting force is parameterized using the waste contact area, pressure and friction characteristics. This remains a simplified system-level representation; it should not be substituted directly for the nonuniform contact-pressure field obtained from Ansys Rocky without calibration.

### 2.2.4 Hydraulic efficiency and energy-based operating criterion

The extended model also represents volumetric efficiency by accounting for leakage relative to pump delivery, and hydraulic efficiency by accounting for pressure losses:

For a pump driven from the vehicle transmission or power take-off, instantaneous hydraulic input power is expressed through the product of pressure and volume flow divided by the hydraulic efficiency:

As a conceptual operating criterion, the extended manuscript proposes minimizing energy expenditure relative to compacted waste mass over a compaction cycle:

This objective could inform a subsequent optimization of pump control, power-take-off operating conditions, and fraction-dependent compaction pressure. However, the present article provides no measured operating cycle, pump efficiency curve, material-specific calibration, or coupled system-level simulation with which to calculate a defensible numerical optimum. The existing structural optimization in this article remains based on press-plate mass, von Mises stress, and Z-direction deflection.

## 2.3 Coupled DEM-FEA model

The computational workflow was implemented in Ansys Workbench and combined Geometry, Rocky Particle Dynamics, Static Structural, Response Surface, and Direct Optimization modules (Fig. 3). The glass compartment was first simulated in Rocky; the resulting contact pressure on the press plate was then imported into Mechanical, where stress and displacement were calculated. The geometric parameters and structural responses were subsequently passed to the response-surface and optimization blocks.

In the DEM model, the compartment was filled with particles representing glass waste and the plate compacted the material through a stroke of 0.6 m (Fig. 4). The adopted contact parameters are listed in Table 2. Friction controls tangential force transfer, while restitution and tangential stiffness influence the contact response. The reported numerical results therefore correspond to this specific parameter set rather than to every possible state of glass cullet.

The imported pressure field is spatially nonuniform (Fig. 5), which is the principal reason for using DEM-derived loading instead of a uniform equivalent pressure. During parametric updates, the load mapping must remain associated with a stable surface or coordinate-based location so that remeshing does not alter the physical loading area.

The finite-element boundary conditions represent the functional guides and hydraulic supports of the plate. Hydraulic-strut constraints act in the Z direction, the 2.8 m side edges are restricted in X, and the 2.5 m edges are restricted in Y (Fig. 6). These idealized constraints are suitable for comparative optimization but should ultimately be checked against the real compliance of the guides, joints, and hydraulic cylinders.

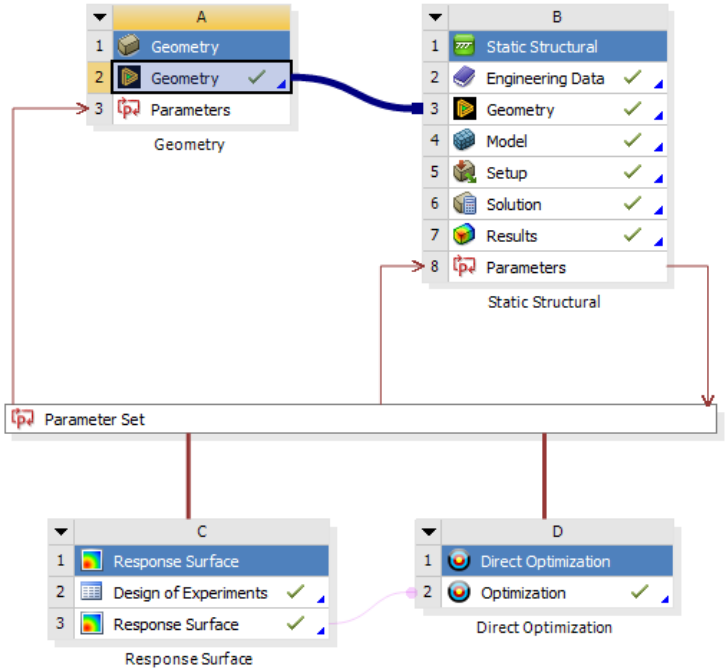



Fig. 3 Coupled Ansys Workbench scheme with Response Surface and Direct Optimization

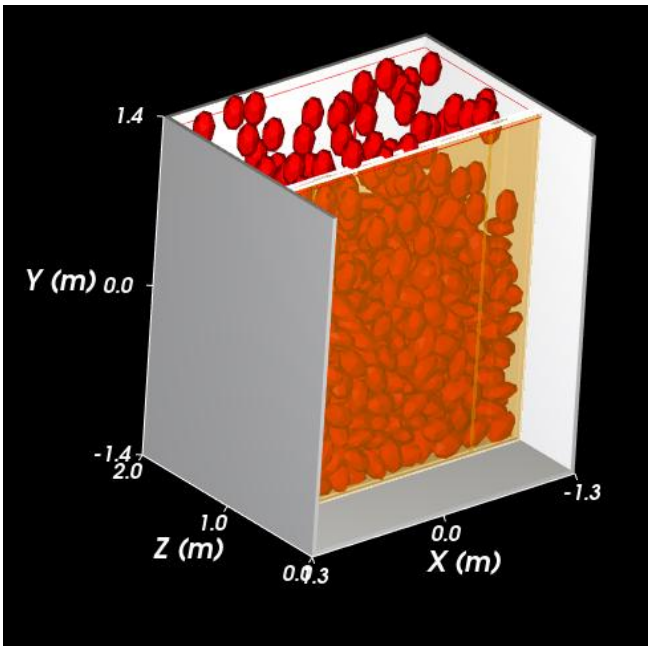



Fig. 4 Glass-waste filling and compaction in Ansys Rocky

## 2.4 Parametric optimization

The optimization domain comprised three independent geometric variables and three structural responses (Table 3). The main-plate thickness t varied from 10 to 50 mm, the hydraulic-strut position a from 100 to 300 mm, and the rib thickness b from 20 to 50 mm. The

outputs were maximum equivalent stress P7, plate mass P9, and minimum Z-direction displacement P10.

Table 2. Contact parameters adopted in the DEM model

| Contact pair | Static friction | Dynamic friction | Tangential stiffness | Restitution |
|---|---|---|---|---|
| Glass-glass | 0.45 | 0.30 | 1.0 | 0.05 |
| Glass-press plate | 0.35 | 0.25 | 1.0 | 0.05 |

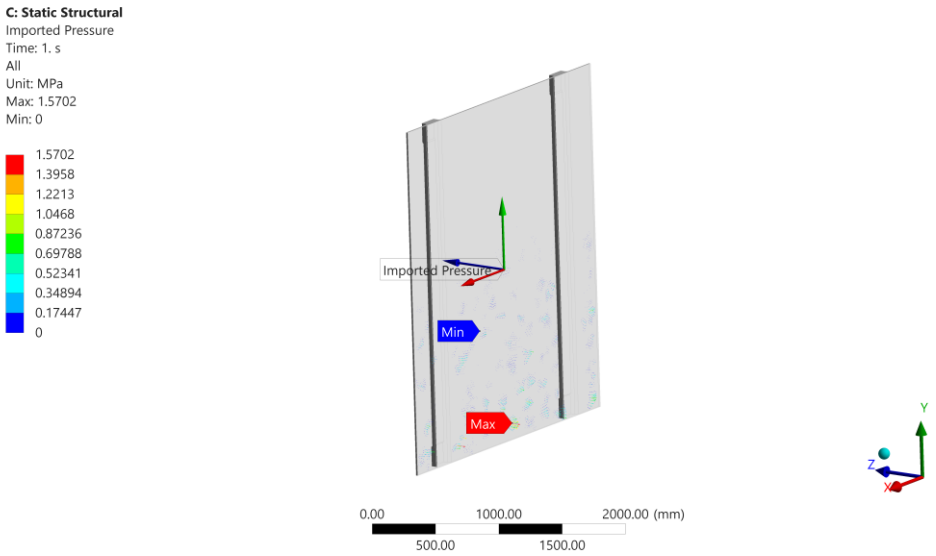



Fig. 5 Imported pressure field from glass waste acting on the press plate

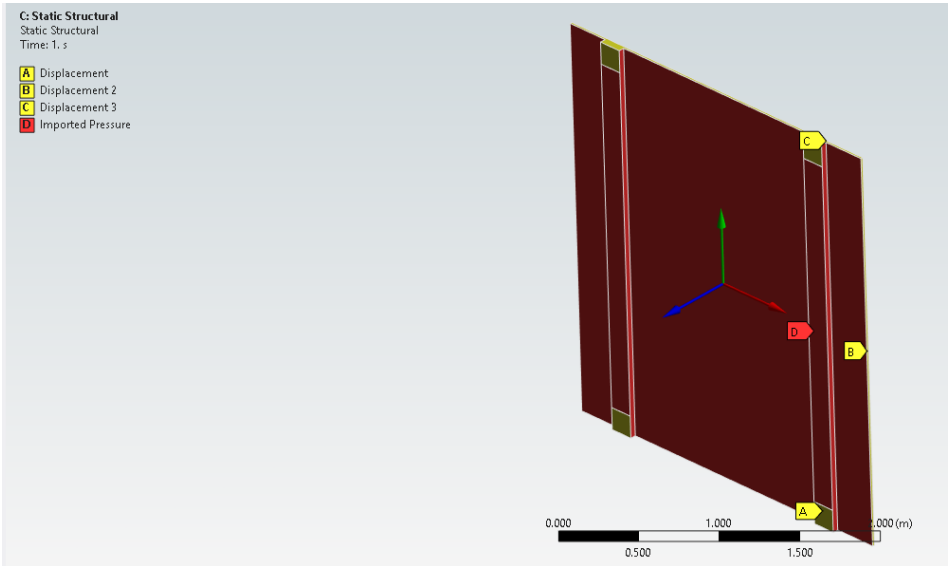



Fig. 6 Boundary conditions of the press-plate finite-element model

Non-Parametric Regression was selected for the response surface because the stress and displacement responses can vary nonlinearly with plate thickness, rib stiffness, and support position. The optimization objective was to minimize mass subject to P7 ≤ 196 MPa and P10 ≥ -8 mm. Thus, stress and displacement were treated as hard constraints, while mass was minimized only within the feasible region.

Table 3. Design variables, responses, and constraints

| Designation | Physical parameter | Range / criterion |
|---|---|---|
| P1-t | Main-plate thickness | 10-50 mm |
| P5-a | Hydraulic-strut attachment position | 100-300 mm |
| P8-b | Stiffening-rib thickness | 20-50 mm |
| P7 | Maximum equivalent stress | ≤196 MPa |
| P9 | Plate mass | Minimize |
| P10 | Minimum Z-displacement | ≥ -8 mm |

## 3 Results and Discussion

### 3.1 Baseline response

For the baseline geometry, the maximum directional displacement along the Z-axis was approximately -10.8 mm (Fig. 7), corresponding to a displacement magnitude greater than the adopted 8 mm limit. The maximum equivalent von Mises stress reached 229.88 MPa (Fig. 8), exceeding the allowable value of 196 MPa. The baseline configuration therefore failed both stiffness and strength criteria and provided a clear basis for parametric optimization.

The negative displacement sign reflects the global coordinate direction in the numerical model; the engineering criterion concerns its magnitude. The optimization problem was consequently formulated to reduce both stress and displacement while avoiding an unnecessary increase in mass.

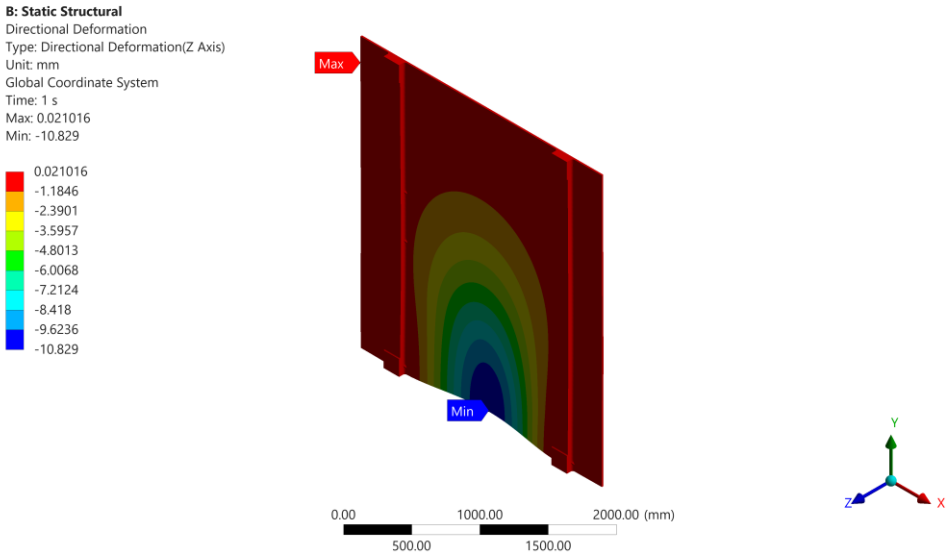



Fig. 7 Directional deformation along the Z-axis for the baseline geometry

### 3.2 Sensitivity and response-surface behavior

The sensitivity analysis indicates that the main-plate thickness t has the strongest influence on stress and displacement (Fig. 9). This result is physically consistent with the strong dependence of bending stiffness on plate thickness. The rib thickness b modifies local and global stiffness with a smaller mass penalty than increasing the entire plate thickness, whereas the support position a changes the reaction-force path and bending-moment distribution.

The response surfaces confirm nonlinear interaction among the variables. At low t, deformation increases sharply, and increasing b cannot fully compensate for insufficient main-plate stiffness (Fig. 10). A similar nonlinear pattern is observed for von Mises stress (Fig. 11): changes in rib thickness can redistribute local stresses, so the lowest stress does not necessarily

occur at the maximum values of all geometric parameters. These trends justify the use of a flexible surrogate rather than a simple linear approximation.

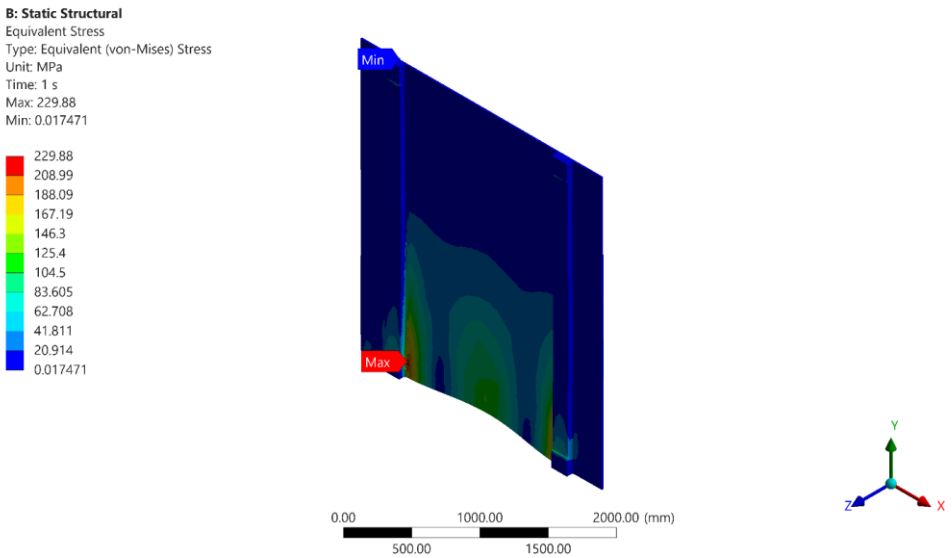



Fig. 8 Equivalent von Mises stress for the baseline geometry

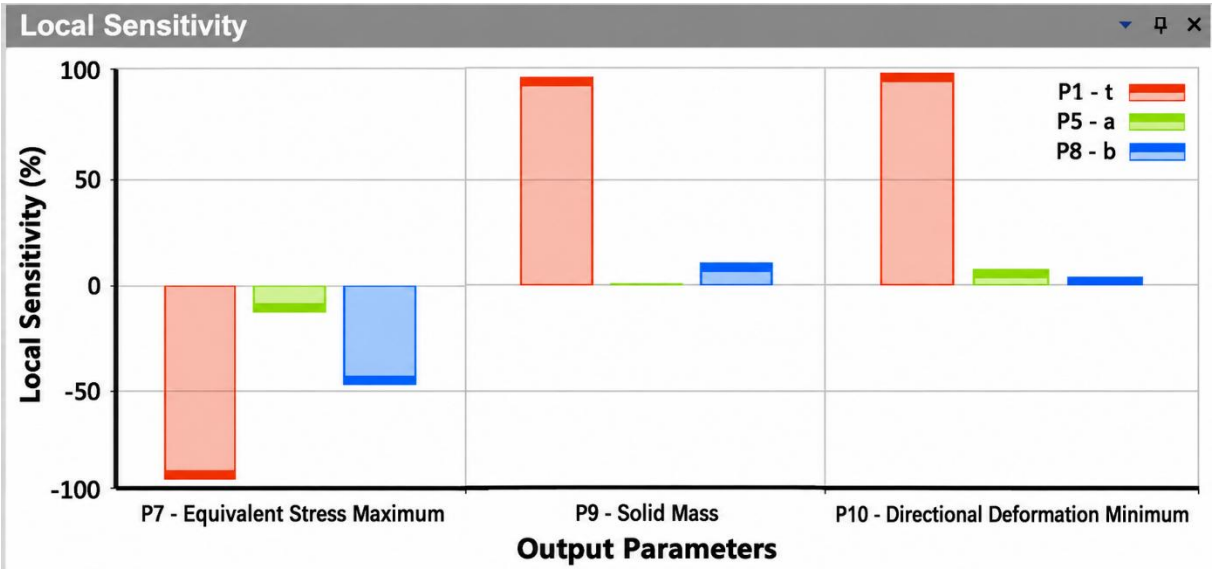



Fig. 9 Sensitivity of design parameters t, a, and b with respect to the calculated outputs

### 3.3 Optimization results and engineering interpretation

The optimization produced three feasible candidate points (Fig. 12 and Table 4). All candidates have a main-plate thickness close to 15 mm but differ in hydraulic-strut position and rib thickness. This indicates that the optimization tends to keep the main plate near a minimum sufficient thickness and uses support placement and rib stiffness to satisfy the constraints.

Candidate Point 1 is the lightest solution, with t = 14.936 mm, a = 283.02 mm, b = 36.877 mm, a maximum stress of 146.81 MPa, a mass of 1072.2 kg, and a displacement of -7.483 mm. It satisfies both constraints and is preferable when minimum mass is the primary objective. Candidate Point 2 increases the mass by only about 11.5 kg but reduces the stress to 110.29 MPa and the displacement magnitude to 6.5934 mm, providing the largest strength margin. Candidate Point 3 is the heaviest of the three and may be useful only if its support position or rib geometry better fits manufacturing constraints.

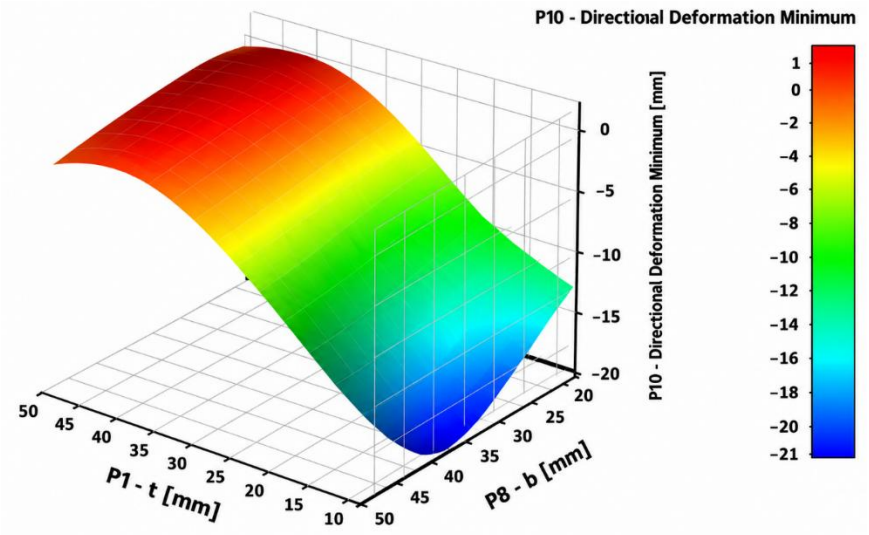



Fig. 10 Response surface of Z-direction displacement as a function of t and b

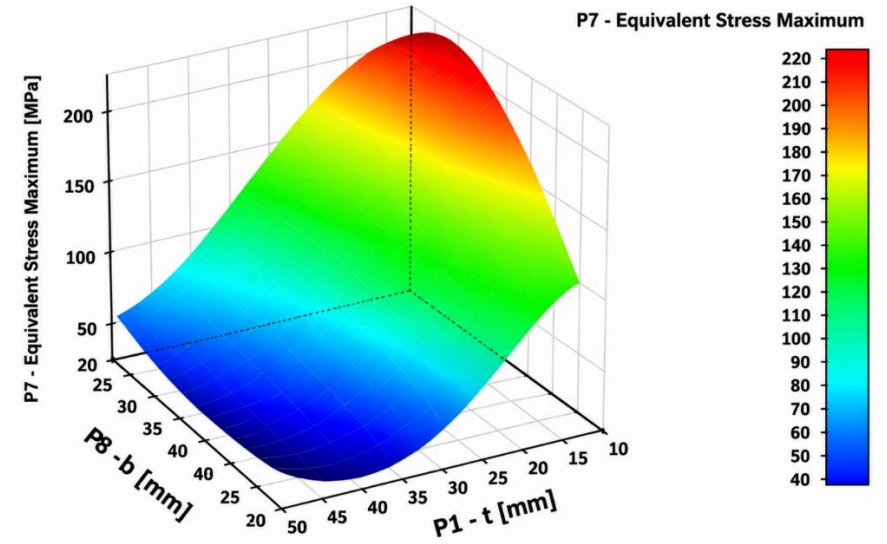



Fig. 11 Response surface of maximum von Mises stress as a function of t and b

From a practical standpoint, the calculated thickness of approximately 14.9 mm can be rounded to a commercially available 15 mm plate, followed by a verification analysis. The final selection should also account for hydraulic-cylinder layout, weld geometry, guide clearances, and manufacturability rather than relying solely on the numerical optimization rank.

The results remain conditional on the adopted DEM and FEA assumptions. A reliable final design should verify conservation of the resultant force during Rocky-to-Mechanical load transfer, demonstrate mesh convergence, and evaluate several particle-size and filling scenarios. DEM contact parameters should be calibrated using a controlled glass-compaction test, while the structural model should be checked experimentally using displacement and strain measurements on a prototype or representative plate segment. These steps are especially important because variations in particle size, packing, friction, and actual support compliance can change local pressure and stress distributions.

Table of Schematic D2: Optimization , Candidate Points

| | A | B | C | D | E | F | G | H | I | J | K |
|---|---|---|---|---|---|---|---|---|---|---|---|
| 1 | Reference | Name | P1 - t (mm) | P5 - a (mm) | P8 - b (mm) | P7 - Equivalent Stress Maximum (MPa) | | P9 - Solid Mass (kg) | | P10 - Directional Deformation Minimum (mm) | |
| 2 | | | | | | Parameter Value | Variation from Reference | Parameter Value | Variation from Reference | Parameter Value | Variation from Reference |
| 3 | ◉ | Candidate Point 1 | 14.506 | 283.02 | 36.877 | 146.81 | 0.00 % | 1072.2 | 0.00 % | -7.483 | 0.00 % |
| 4 | ○ | Candidate Point 2 | 14.806 | 240.79 | 37.597 | 110.29 | -24.88 % | 1093.7 | 2.01 % | -6.5934 | 11.89 % |
| 5 | ○ | Candidate Point 3 | 14.603 | 220.52 | 39.905 | 122.95 | -16.25 % | 1098.8 | 2.48 % | -6.9906 | 6.58 % |
| * | | New Custom Candidate Point | 30 | 200 | 35 | | | | | | |

Fig. 12 Candidate points obtained by Direct Optimization

Table 4. Comparison of feasible optimization candidates

| Candidate | t, mm | a, mm | b, mm | Stress, MPa | Mass, kg | P10, mm |
|---|---|---|---|---|---|---|
| Point 1 | 14.936 | 283.02 | 36.877 | 146.81 | 1072.2 | -7.483 |
| Point 2 | 14.886 | 240.79 | 37.597 | 110.29 | 1083.7 | -6.5934 |
| Point 3 | 14.603 | 220.52 | 39.905 | 122.95 | 1098.8 | -6.9906 |

## CONCLUSIONS

A coupled DEM-FEA methodology was developed for strength assessment and parametric optimization of the glass-compartment press plate in a variable-volume three-compartment refuse collection vehicle. DEM simulation in Ansys Rocky provided the nonuniform contact pressure generated during glass compaction, and the transferred load was evaluated in Ansys Mechanical.

The baseline design failed the adopted criteria, with a maximum Z-direction displacement of approximately -10.8 mm and a maximum von Mises stress of 229.88 MPa. Parametric optimization of t, a, and b identified three feasible designs satisfying P7 ≤ 196 MPa and P10 ≥ -8 mm.

The minimum-mass candidate had t = 14.936 mm, a = 283.02 mm, b = 36.877 mm, a stress of 146.81 MPa, a mass of 1072.2 kg, and a displacement of -7.483 mm. A second candidate offered a larger strength margin with only a small mass increase, demonstrating that final design selection can balance mass, structural reserve, and manufacturability.

Before practical implementation, the optimized geometry should be rounded to available manufacturing dimensions and reanalyzed. Experimental calibration of DEM contact parameters, verification of load-transfer consistency and mesh convergence, and structural validation of the plate-support system are required. The same computational framework can subsequently be adapted to the plastic and paper compartments using fraction-specific material models.

## REFERENCES


[1] Myers, R. H., Montgomery, D. C., Anderson-Cook, C. M. "Response Surface Methodology: Process and Product Optimization Using Designed Experiments", Wiley, **2016**.

[2] Simpson T. W., Mauery, T. M., Korte, J. J., Mistree, F. "Kriging models for global approximation in simulation-based multidisciplinary design optimization", AIAA Journal 39, pp. 2233 – 2241, **2001**.

[3] EP0790194A1, "Refuse collection and compaction vehicle, European Patent Application".

[4] Kadyrov, A .S., Karsakova A. Zh., Donenbayev, B. S., Balabekova, K. "Establishing the strength characteristics of the lifting-leveling device structures of the VPO-3-3000 machines for the track straightening", Communications - Scientific Letters of the University of Žilina 22 (4), pp. 70 – 79, **2020**.

[5] Kadyrov, A. S., Pak, I. A., Ganyukov, A., Imanov, M. O., Balabekova, K. "Research of operation of equipment for ultrasonic purification of exhaust gases of internal combustion engines", Journal of Engineering Physics and Thermophysics 94 (6). pp. 1407 – 1414, **2021**.

[6] Kizdarbekova, M., Balabekova, K., Zabiyev, A., Konyrtaeva, K. "Improvement of the body structure for efficient collection of municipal waste", Eurasian Journal of Applied Engineering and Technology (EJAET) 155 (2), pp. 163 – 172, **2026**. DOI: 10.32523/3136-3385-2026-155-2-163-172

[7] Jebahi, M., Dau, F., Iordanoff, I., Guin, J.-P. "Virial stress-based model to simulate the silica glass densification with the discrete element method", International Journal for Numerical Methods in Engineering 112 (13), pp. 1909 – 1925, **2017**. DOI: 10.1002/nme.5589

[8] Roux, W. J., Stander, N., Haftka, R. T. "Response surface approximations for structural optimization", International Journal for Numerical Methods in Engineering 42 (3), pp. 517 –534, **1998**. DOI: 10.1002/(SICI)1097-0207(19980615)42:3<517::AID-NME370>3.0.CO;2-L

[9] Kenesbek, I., Togizbayeva, B. B., Balabekova, K., Sazambayeva, B. T. "Improvement of Crane Efficiency via Design Optimization", Strojnícky časopis – Journal of Mechanical Engineering 76 (1), pp. 71 – 78, **2026**. DOI: 10.2478/scjme-2026-0006

[10] Danyarova, A., Togizbayeva, B. B., Balabekova, K., Vlnka, J. "Investigation of Strength and Calculation of Wear Resistance of a Quick-Release Mechanism in Connection With the Working Attachment of a Hydraulic Excavator", Strojnícky časopis – Journal of Mechanical Engineering 75 (1), pp. 9 – 16, **2025**. DOI: 10.2478/scjme-2025-0002

[11] Togizbayeva, B. B., Zabiyeva, A. B., Balabekova, K., Kenesbek, A. B. "Development of a Calculation Method for Determining the Permissible Dimensions of the Defect 11", Acta Polytechnica Hungarica 20 (4), pp. 249 – 267, **2023**. DOI: 10.12700/APH.20.4.2023.4.14

[12] Lolov, D., Lilkova-Markova, S. "The Model of Interconnected Pipes in the Investigation of Dynamic Stability of Carbon Nanotubes Embedded in an Elastic Medium", Strojnícky časopis – Journal of Mechanical Engineering 73 (2), pp. 93 – 98, **2023**. DOI: 10.2478/scjme-2023-0024

[13] Choudhury, A., Chandra, S., Sarkar, S., & Karmakar, M. "Analysis of Simply Supported Laminated Composite Plate by Semi Analytical and Finite Element Method for Different Orientation Angles", Strojnícky časopis – Journal of Mechanical Engineering 73 (2), pp. 45 – 70, **2023**. DOI: 10.2478/scjme-2023-0021

[14] Baťa, M., Lazorík, A., Mazúr, S. "Design and Manufacturing of a High-Performance Battery Module for an Electric Racing Vehicle", Strojnícky časopis – Journal of Mechanical Engineering 75 (2), pp. 1 – 20, **2025**. DOI: 10.2478/scjme-2025-0019

[15] Szeliga, J., Kohut, J., Pleva, L., Frydrýšek, K., Čepica, D. "Measurement of Dosed Compression and Distraction of Tibia Fractures Treated with Ilizarov Circular External Fixation", Strojnícky časopis – Journal of Mechanical Engineering 75 (2), pp. 97 – 110, **2025**. DOI: 10.2478/scjme-2025-0027

[16] Welch, M. "Bolted Joint Preload Distribution from Torque Tightening", Strojnícky časopis – Journal of Mechanical Engineering 71 (2), pp. 329 – 342, **2021**. DOI: 10.2478/scjme-2021-0039

[17] Bider, Zs., "Influence of the Tolerances of the Threaded Joints on Preloaded Bolted Connection", Strojnícky časopis – Journal of Mechanical Engineering 75 (1), pp. 173 – 178, **2025**. DOI: 10.2478/scjme-2025-0018

[18] Dung, H. T., Do, D. T., Nguyen, V. T. "Comparison of Multi-Criteria Decision Making Methods Using The Same Data Standardization Method", Strojnícky časopis – Journal of Mechanical Engineering 72 (2), pp. 57 – 72, **2022**. DOI: 10.2478/scjme-2022-0016

[19] Pham, Q. M., Vu, V. T., Tran, L. Q., Nguyen, H. H., & Hong, T. D. "Study on Kinetics and Dynamics of the Scraping-Pressing Mechanism of the Compactor Garbage Truck", FME Transactions, 52(4), pp. 603 – 615, **2024**. DOI: 10.5937/fme2404603q